Received: 6 May 2024 | Revised: 13 August 2024 | Accepted: 26 August 2024

DOI: 10.1002/alz.14266

Alzheimer's & Dementia®
THE JOURNAL OF THE ALZHEIMER'S ASSOCIATION

RESEARCH ARTICLE

Sex-specific topological structure associated with dementia via latent space estimation

Selena Wang[1] | **Yiting Wang**[2] | **Frederick H. Xu**[3] | **Xinyuan Tian**[4] | **Carolyn A. Fredericks**[5] | **Li Shen**[6] | **Yize Zhao**[4] | **for the Alzheimer's Disease Neuroimaging Initiative**

[1]Department of Biostatistics and Health Data Science, Indiana University School of Medicine, Indianapolis, Indiana, USA

[2]Department of Statistics, University of Virginia, Charlottesville, Virginia, USA

[3]Department of Bioengineering, University of Pennsylvania, Philadelphia, Pennsylvania, USA

[4]Department of Neurology, Yale School of Medicine, Yale University, New Haven, Connecticut, USA

[5]Department of Biostatistics, Epidemiology and Informatics, University of Pennsylvania, Philadelphia, Pennsylvania, USA

[6]Department of Biostatistics, Yale School of Public Health, New Haven, Connecticut, USA

Correspondence
Selena Wang, Department of Biostatistics and Health Data Science, Indiana University School of Medicine, 410 West 10th Street, Suite 3000, Indianapolis, IN 46202, USA.
Email: selewang@iu.edu

Data used in preparation of this article were obtained from the Alzheimer's Disease Neuroimaging Initiative (ADNI) database (adni.loni.ucla.edu). As such, the investigators within the ADNI contributed to the design and implementation of ADNI and/or provided data but did not participate in the analysis or writing of this report. A complete listing of ADNI investigators can be found at: http://adni.loni.usc.edu/wp-content/uploads/how_to_apply/ADNI_Acknowledgement_List.pdf.

Funding information
Alzheimer's Disease Neuroimaging Initiative; National Institutes of Health, Grant/Award Number: U01 AG024904; Department of Defense, Grant/Award Number: W81XWH-12-2-0012; National Institute on Aging; National Institute of Biomedical Imaging and Bioengineering, Grant/Award Numbers: R01EB034720, RF1AG068191, RF1AG081413

Abstract

INTRODUCTION: We investigate sex-specific topological structures associated with typical Alzheimer's disease (AD) dementia using a novel state-of-the-art latent space estimation technique.

METHODS: This study applies a probabilistic approach for latent space estimation that extends current multiplex network modeling approaches and captures the higher-order dependence in functional connectomes by preserving transitivity and modularity structures.

RESULTS: We find sex differences in network topology with females showing more default mode network (DMN)-centered hyperactivity and males showing more limbic system (LS)-centered hyperactivity, while both show DMN-centered hypoactivity. We find that centrality plays an important role in dementia-related dysfunction with stronger association between connectivity changes and regional centrality in females than in males.

DISCUSSION: The study contributes to the current literature by providing a more comprehensive picture of dementia-related neurodegeneration linking centrality, network segregation, and DMN-centered changes in functional connectomes, and how these components of neurodegeneration differ between the sexes.

KEYWORDS
Alzheimer's disease, connectome-driven degeneration, epicenter progression hypothesis, network segregation, network topology, network-based neurodegeneration

Highlights

- We find evidence supporting the active role network topology plays in neurodegeneration with an imbalance between the excitatory and inhibitory mechanisms that can lead to whole-brain destabilization in dementia patients.
- We find sex-based differences in network topology with females showing more default mode network (DMN)-centered hyperactivity, males showing more limbic system (LS)-centered hyperactivity, while both show DMN-centered hypoactivity.
- We find that brain region centrality plays an important role in dementia-related dysfunction with a stronger association between connectivity changes and regional centrality in females than in males.
- Females, compared to males, tend to exhibit stronger dementia-related changes in regions that are the central actors of the brain networks.
- Taken together, this research uniquely contributes to the current literature by providing a more comprehensive picture of dementia-related neurodegeneration linking centrality, network segregation, and DMN-centered changes in functional connectomes, and how these components of neurodegeneration differ between the sexes.

1 | BACKGROUND

Sex is an important biological indicator of Alzheimer's disease (AD) and related dementias (ADRD). More women are impacted by AD than men.[1] Women tend to experience faster rates of neuronal deterioration and atrophy than men.[2,3] Neuroimaging methods, for example, resting-state functional magnetic resonance imaging (rs-fMRI), have been used to identify sex differences in functional co-activation patterns between AD patients and healthy participants. Early research shows evidence in sex-specific spatial pattern correspondence between intrinsic functional connectivity networks and neurodegenerative atrophy patterns[4] revealing links between dementia-induced atrophy and irregularities in functional connectivity.

Network-based neurodegeneration model hypothesizes that connections in the brain act as conduits for the propagation of pathological proteins with accumulation along brain connections.[5–8] It suggests that pathological proteins originate at disease epicenters and then spread across the whole brain.[9] The epicenter progression hypothesis has gained support in the literature with positive associations found between connectivity strength and pathology[10,11] and protein aggregation found between brain regions with strong anatomical connections.[5,6] The latter has also gained support in longitudinal studies with a faster rate of protein aggregation in regions connected to epicenters.[12,13] Specific attention has been given to the default mode network (DMN), a set of co-activating brain regions with a non-trivial overlap with β-amyloid[14–19] deposition. To differentiate co-activating clusters of brain regions, for example, DMN from whole-brain connectivity, we call the former circuits and the latter brain networks in the current study. Because the whole-brain connectivity is the more complete network, functional circuits can be seen as local clusters that play crucial roles in the whole-brain network.

Recent evidence suggests that the interconnected nature of the brain plays a more active role in degeneration than has been indicated in the epicenter progression hypotheses,[9] pointing to changes in the network topology—logical and relational arrangements of the brain nodes and connections. The connectome-driven degeneration model hypothesizes that the accumulation of pathological protein may first interfere with the information flow via connected regions locally, but can ultimately create an imbalance between excitatory and inhibitory mechanisms, leading to whole-network destabilization.[20,21] Although networks are often found be efficient for information communication and resilient to local dysfunctions, the literature also points to the presence of the tipping point, bypassing of which can lead to a whole-system collapse.[20,22–24] One aspect of topology in brain networks, network segregation and integration, the relative intensity in within-circuits connectivity to between-circuits connectivity, is a key indicator of instability.[25–27] Evidence supports a loss of network segregation during aging, with growing connectivity between functional circuits and weakening connectivity within each functional circuit as we age. This imbalance can result in a less efficient whole-brain connectivity network, exacerbating neurodegeneration and cognitive decline.[20,21,28]

Despite the critical role topology plays in neurodegeneration, there is a lack of studies investigating whole-brain topology in neurodegeneration while pinpointing localized sex-specific dysfunction at the node or circuit level. Regional investigations can provide insights into the roles that key regions and circuits such as DMN play in dysfunction, but there are downsides as well. First, investigations at the circuit level often assume the stability of functional circuits between healthy and dementia patients though evidence supports heterogeneity in functional circuits across participants and the mixing of region-to-circuit membership across the human lifespan.[29–31] In addition, functional circuits and protein composition only show moderate spatial matching,[15,32] which may suggest that functional circuits do not provide the whole picture for protein spread and are only a part of the whole-brain communication feature. Further investigation is needed. Brain hubs, for example, are known to transmit information across functional circuits.[33] Ultimately, the brain is a complex network containing connections within and between circuits, and studying only pieces of the network does not give a holistic picture of the sex differences in brain function and degeneration. The applications of statistical network analytical techniques to neuroimaging have allowed us to address this gap and investigate the whole-brain differences while preserving network modularity. For AD research, modularity plays an important role in degeneration. The DMN, for example, is a key in AD pathology. AD patients tend to show impaired DMN activity in the early symptomatic stage,[34–37] and DMN regions are consistently found with tau deposition.[4,38]

We apply a novel latent space joint network model[39] to perform a case–control comparison using the functional connectivity data together with region-specific cortical volume, cortical thickness, surface area, and positron emission tomography (PET) information. We apply our model to males and females separately to identify potential sex differences in functional imaging biomarkers of dementia[26,27] and uncover sex-specific topological structures associated with dementia.

We find evidence supporting the active role network topology plays in neurodegeneration, an imbalance between excitatory and inhibitory mechanisms that accelerates whole-brain destabilization in dementia patients. We find sex-based differences in network topology with females showing more DMN-centered hyperactivity and males showing more limbic system (LS)-centered hyperactivity, while both show DMN-centered hypoactivity. Centrality plays an important role in dementia-related dysfunction with a stronger association between connectivity changes and regional centrality in females than in males. Females, compared to males, tend to exhibit stronger dementia-related changes in regions that are the central actors of the brain networks.

RESEARCH IN CONTEXT

1. **Systematic review**: We investigate sex-specific topological structure associated with typical Alzheimer's disease (AD) dementia using a novel state-of-the-art latent space estimation technique. We apply a probabilistic approach for latent space estimation that extends current multiplex network modeling approaches and captures the higher-order dependence in functional connectomes by preserving transitivity and modularity structures.
2. **Interpretation**: We find sex differences in network topology with females showing more default mode network (DMN)-centered hyperactivity and males showing more limbic system (LS)-centered hyperactivity, while both show DMN-centered hypoactivity. We find that centrality plays an important role in dementia-related dysfunction with a stronger association between connectivity changes and regional centrality in females than in males.
3. **Future directions**: Future studies should extend the current study and provide a more comprehensive picture of dementia-related neurodegeneration linking centrality, network segregation, and DMN-centered changes in functional connectomes and further investigate how these components of neurodegeneration differ between the sexes.

2 | METHODS

2.1 | Participants

Data used in the preparation of this article were obtained from the Alzheimer's Disease Neuroimaging Initiative (ADNI) database (adni.loni.usc.edu). The ADNI was launched in 2003 as a public–private partnership, led by Principal Investigator Michael W. Weiner, MD. The primary goal of ADNI has been to test whether serial magnetic resonance imaging (MRI), PET, other biological markers, and clinical and neuropsychological assessment can be combined to measure the progression of mild cognitive impairment (MCI) and early AD.[40]

Participants were from the third release of the ADNI study including 211 males and 199 females, a sample size of 410 in total. To be included in our study, subjects must have both structural MRI (sMRI) and rs-fMRI scans at enrollment or year-1 time points with baseline scans in two modalities. Participants self-identified their sex as male or female. Of these, 196 participants were healthy, 157 participants showed MCI, and 57 participants showed symptoms of typical AD dementia. The AD dementia participants are hereon referred to as the dementia group, per the ADNI-3 dataset diagnostic label.[40]

See the demographic information across three clinical groups in Table 1. Across the three clinical groups, we found comparable demographic information regarding sex and race. We found a comparable age range across three clinical groups with differences in the average age of the participants. This result is expected because age is the key risk factor for developing ADRD, and it makes sense that dementia patients tend to be older than MCI and healthy participants.

2.2 | PET

Preprocessed florbetapir (AV45) and florbetapen (FBB) PET data were obtained from ADNI3, using the UC Berkeley PET Imaging

TABLE 1 Demographic information for different clinical groups

Parameter	Healthy ($N = 196$)	MCI ($N = 157$)	Dementia ($N = 57$)
Sex			
Female	102 (52.0%)	73 (46.5%)	24 (42.1%)
Male	94 (48.0%)	84 (53.5%)	33 (57.9%)
Age			
Mean (SD)	70.7 (6.6)	71.8 (7.1)	74.4 (7.1)
Range	55.5–87.4	55.0–89.1	56.7–89.2
Race			
American Indian/Alaskan	1 (0.5%)	0 (0.0%)	0 (0.0%)
Asian	1 (0.5%)	2 (1.3%)	1 (1.8%)
Black	13 (6.6%)	3 (1.9%)	0 (0.0%)
More than one	4 (2.0%)	2 (1.3%)	1 (1.8%)
White	176 (89.8%)	149 (94.9%)	55 (96.5%)
Unknown	1 (0.5%)	1 (0.6%)	0 (0.0%)

Abbreviation: MCI, mild cognitive impairment; SD, standard deviation.

Dataset.[41,42] The PET data were first date-matched to the fMRI scans for each subject, selecting the PET scan that was closest to the fMRI scan in acquisition date. The data contain standardized uptake value ratio (SUVR) values for cortical regions of the Desikan–Killiany Atlas from the two types of imaging tracers. To harmonize the data, each tracer's SUVR values were converted to the centiloid (CL) scale for consistency.[43] Due to the cross-sectional design of the present study, the normalization process in the conversion was done concerning the cerebellum's SUVR for each tracer type. The CL values were then used for subsequent analysis.

2.3 | rs-fMRI data

Image processing was performed according to procedure outlined in a previous paper,[44] conducted using the ConnectomeMapper3 pipeline,[45] which consolidates several open-source packages for brain registration, segmentation, and blood oxygen level-dependent (BOLD) time signal processing. The sMRI volumes were first segmented using FreeSurfer's reconall function before being parcellated using Scale 1 of the Lausanne 2018 parcellation.[46] For rs-fMRI preprocessing, the images underwent despiking and slice timing correction using AFNI[47] and motion correction and distortion correction using FSL. Each subject's rs-fMRI images were then registered to their corresponding b0 sMRI volumes using the FLIRT toolbox in FSL.[48,49] The BOLD time signals of each region of interest (ROI) were then band-pass filtered and detrended using linear regression. Global signal regression was not applied for this study.[27] Functional brain networks were constructed for each subject by computing the Pearson correlation between the BOLD time signals of pairs of ROIs. We excluded the subcortical regions and focused on cortical regions for study, resulting in networks with 68 regions in size. These 68 cortical regions of the Lausanne 2018 atlas matched those of the Desikan–Killiany atlas. Last, we performed two mappings between the regions and subsystem labels: the seven Resting-State Functional Subnetworks (RSNs) and subcortical regions from the Yeo Atlas[50] and anatomical lobe mappings from FreeSurfer.[51] These mappings allow for the observation of higher-order dysfunction at a subsystem level.

In addition, we downloaded regional anatomical measurements from the University of California San Francisco FreeSurfer 5.1 Cross-Sectional Study database, and the same processing procedures were performed.[39] We included the cortical attributes, cortical volume, surface area, and average thickness.

2.4 | Latent space estimation

Investigations of connectomes via latent space dimensions or gradients have seen a surge of applications in the literature.[52–57] This study applies a probabilistic approach for latent space estimation called attributes informed brain connectivity (ABC) estimation.[39] We briefly reiterate here to demonstrate its applicability with functional connectomes, MRI, and PET modalities.

Suppose we have latent space dimensions Z, X, and Y that represent meaningful information in MRI derived regional cortical volume, thickness and surface area (Z), PET-derived SUVR values (X), and fMRI derive functional connectomes (Y). Instead of estimating latent connectivity dimensions Y using matrix factorization methods, and then linking functional connectomes with PET and MRI, we can, in one wholistic generative model, estimate Z, X, and Y simultaneously with a shared distribution. To achieve this objective, we formulate the model into two components, latent-space estimation of brain connectivity and data-driven integration of the brain region-level information including MRI-derived regional cortical volume, thickness, and surface area as well as PET-derived SUVR values.

For subject i ($i = 1,\ldots, N$), we use $A_i \in \mathrm{R}^{V\times V}$ to denote the network phenotype in the form of a V by V adjacency matrix. Stacking A_i across all the subjects, we have the network array $\mathrm{A}\in\mathrm{R}^{V\times V\times N}$. In this study, we derive the network phenotype using fMRI data, resulting in A_i being a symmetric functional connectome matrix for each subject with diagonal elements as zero. For subject i ($i = 1,\ldots, N$), we use $B_i \in R^{V\times 4}$ to denote the multivariate matrix containing brain region-level information: (1) cortical volume, (2) thickness, and (3) surface area, as well as (4) PET-derived SUVR values. We formulate the model as follows.

$$A_i = \varphi_i + ZZ^T + E_i, \tag{1}$$

$$B_i = \theta_i + [X, Y] + \Psi_i, \tag{2}$$

where Z is the V by K latent connectivity matrix, each row of which, z_v contains the meaningful (without noise) connectivity information for node v, $z_v \in R^K$, $K \ll V$; ϕ_i is the fixed intercept accounting for individual overall connectivity variation; E_i is the V by V symmetric error matrix, each element of which is $e_{v,v',i}, v < v', v, v' = 1,2,..,V$, $e_{v,v',i} \overset{iid}{\sim} N(0,\sigma^2)$, and σ^2 is the error variance; X is the V by three regional MRI information matrix, each row of which, x_v contains the meaningful (without noise) cortical volume, thickness and surface area information for node v; Y is the V by one PET matrix, each row of which, y_v contains the meaningful (without noise) PET-derived SUVR values information for node v; θ_i is the fixed intercept accounting for individual attribute variation; Ψ_i is the V by four error matrix, each element of which is $\epsilon_{v,p,i}$, $\epsilon_{v,p,i} \overset{iid}{\sim} N(0,\tau^2)$, and τ^2 is the error variance.

We used a non-informative prior for the covariance matrix Σ. The reason is that we aim to assess the relationship between connectivity and regional attributes in a data-driven fashion, the non-informative prior for the covariance matrix allows us to assess whether the dependence between connectivity and regional attributes exists without being biased by prior knowledge. In particular, we assigned a Wishart $(I_{K+4}, K+4+2)$ prior distribution for $\boldsymbol{\Sigma}$, facilitating a nonzero posterior correlation between brain connectivity and node-level attributes. When the PET-derived SUVR values are significantly related to brain connectivity, the associated covariance estimate should be significantly different from zero based on its posterior distribution. The approximation of the posterior distributions for the unknown quantities is facilitated by setting noninformative priors including a gamma(1/2,1/2) distribution for $\sigma_e{}^{-2}$ and a N(0,1) distribution for a_i. Similarly, N(0,1) and gamma (1/2,1/2) prior distributions are assigned for b_i and $\tau_i{}^{-2}$, respectively.

We used symmetric bilinear effects to capture the higher-order dependence in the connectivity network preserving transitivity and modularity structures.[58–61] Multiplicative effects such as the bilinear effects models, capture clusterability of network structures, and networks with varying degrees of clusterability can be well fitted by such models.[58] Given the small-world properties of functional connectomes,[62] likely exhibiting both transitivity and clusterability, bilinear effects are optimal.

We estimated group-level connectivity latent space across all subjects, and the different persons' connectivity share the same set of nodes. We model dependence across different layers (each layer represents information from one participant) using a shared set of latent variables. This approach is validated in the latent space joint model,[63,64] and the authors, who propose a shared set of latent variables across layers, assuming a joint relational structure across sets of networks. Such an approach has been demonstrated to capture dependence across layers and improve the overall predictive power of the model. We capture the associations between functional connectomes with PET and MRI via the covariance of the latent dimensions, $\boldsymbol{\Sigma}$. Regional attributes are modeled mirroring the modeling of the connectivity with exceptions because connectivity and regional attributes have different dependence structures that warrant different modeling approaches.

Last, but not least, we propose to estimate Z, X, and Y simultaneously as follows: $(z_v, x_v, y_v)^T \overset{iid}{\sim} MVN\left(\begin{pmatrix}0_K\\0_3\\0\end{pmatrix}, \Sigma\right)$, where $\boldsymbol{\Sigma}$ is the $(K+4)\times(K+4)$ covariance matrix for the brain connectivity, MRI derives regional metrics and PET-derived SUVR values. When there are nonzero elements in the off-diagonal matrix of $\boldsymbol{\Sigma}$ matrix, the connectivity and node attribute estimations are dependent, and they regulate and inform each other during model estimation.

The ABC model extends current multiplex network modeling approaches[63,64] to analyze multiple layers of functional networks with a shared set of regions across the whole brain. It improves the current latent space estimation algorithms via multimodality integration, borrowing regional MRI and PET measurements to improve group-level functional connectivity estimation with uncertain quantification. True latent space dimensions reflecting meaningful functional connectome information are separated from random noisy variations, and the model allows latent space dimensions of multiple imaging modalities, PET, fMRI, and MRI to covary across brain regions with the degree of covariation estimated via the model.

Given the above complexities, the model cannot be estimated by existing software. We detail a novel Bayesian Markov chain Monte Carlo (MCMC) algorithm to estimate the proposed joint model.[39] The Bayesian algorithm estimates model parameters in an iterative fashion, and with sufficient iterations, stable Markov chains can be obtained to approximate various quantities of the targeted posterior distributions, which allows uncertainty quantification. Each model was fitted with 500,000 iterations with a burn-in period of 500 and thinning every tenth sample. Each model took about 30 h to complete with 3.11 GB memory and one computing node with one core on the Yale HPC cluster. We found no obvious signs of non-convergence in trace plots; see examples in the Supplementary Material.

3 | RESULTS

We estimated the group-level (including dementia female, dementia male, MCI female, MCI male, healthy female, and healthy male) functional connectivity while incorporating the brain node attributes information on the cortical volume, surface areas, average cortical thickness, and PET. Each of the six groups has 24, 33, 73, 84, 102, and 94 participants, respectively; the differences in sample sizes

TABLE 2 Out-of-sample predictive accuracy with different latent space dimensions.

	Female			Male		
Dimension	Healthy	MCI	Dementia	Healthy	MCI	Dementia
2	0.391	0.402	0.417	0.445	0.412	0.417
3	0.501	0.462	**0.466**	0.504	0.478	**0.483**
4	0.533	0.495	0.312	0.539	0.505	0.120
5	**0.562**	**0.539**	0.352	**0.565**	**0.539**	0.156
6	0.515	0.525	0.118	0.526	0.512	0.109
7	0.122	0.142	0.164	0.131	0.178	0.149
8	0.111	0.135	0.127	0.119	0.099	0.115

Note: The optimal dimension for the data was bolded.
Abbreviation: MCI, mild cognitive impairment.

were addressed within the Bayesian framework in the uncertainty of the parameter estimation with approximated posterior distributions. Subsequent pairwise case–control comparisons were conducted to identify connectivity changes associated with the development of MCI and dementia and to determine whether such changes exhibit sex-based differences.

We found multiple aspects of dementia-related sex differences in functional connectivity changes. First, while dementia patients tended to show changes in functional connectivity across the whole brain, participants with MCI tended to show more local dysfunctions. Second, while both males and females exhibited significant loss of connectivity in the DMN, females showed more DMN-centered hyperconnectivity, whereas males showed more LS-centered hyperconnectivity. Last, we observed a stronger association between connectivity changes and regional centrality in females than in males. Females, compared to males, tended to exhibit stronger dementia-related changes in regions that are the central actors of the brain networks.

3.1 | Model performance

The quality of fit of the model to data was evaluated based on the out-of-sample predictive performance. We evaluated the out-of-sample predictive performance under different numbers of dimensions as follows:

1. We randomly divided the participants into three sets: training (n—8 subjects, where n is the group size), validation (average 5%), and test set (average 10%).
2. For each number of dimensions equaling 2, 3, 4, 5, 6, 7, 8, we fitted the training data to the ABC model.
3. We captured the group-level connectivity using the posterior mean of the estimated latent connectivity variables in the training data.
4. We compared the fit of the model with varying numbers of dimensions using the correlation between the predicted and the observed connectivity in the evaluation set.

We repeated the process 10 times. Table 2 shows the results of the average out-of-sample prediction accuracy values on the evaluation data when the number of dimensions is from 2 to 8. The results showed that the predictive power increased as the number of dimensions increased from two to five for MCI female, MCI male, healthy female, and healthy male participants, and then decreased as the number of dimensions continued to increase, the highest predictive power was observed with five dimensions. For dementia female and dementia male subjects, the predictive power increased as the number of dimensions increased from two to three; the highest predictive power was observed with three dimensions. The prediction accuracy values with five dimensions for MCI and healthy participants and three dimensions for dementia participants showed a satisfactory fit of the ABC model to the data. The prediction accuracy with selected dimensions shows similar values using the test data.

3.1.1 | Less variable functional connectivity is found in dementia patients

From the stabilized MCMC chains (see examples in the Supplementary Materials), we obtained 95% posterior credible intervals (95% CIs) for each of the estimated connectivity edges. We considered a functional brain connectivity edge to be significant when the 95% CI does not contain zero, significantly positive when the lower bound is above zero, and significantly negative when the upper bound is below zero. We depict the estimated whole-brain functional connectivity networks for males and females in Figure 1A and Figure 2A. The associated 95% CIs for connectivity edges in DMN, which is often found to be implicated in neurodgeneration,[26,65,66] are reported in Figure 1B and Figure 2B for males and females. Connectivity edges are ranked by their sizes; large positive edges are ranked high on the y-axis and large negative edges are ranked low on the y-axis from the baseline healthy female participants. The DMN and other circuits are mapped based on the seven RSNs and subcortical regions from the Yeo Atlas.[50] In Figure 1B and Figure 2B, we also added the line $x = 0$ for easier identification of significant and nonsignificant edges. This allows us to demonstrate whether the 95% CI for the connectivity edges of healthy, dementia, and MCI participants includes zero or not.

We added a red star for each significantly different connectivity edge in Figure 1B and Figure 2B, where there is no overlap between

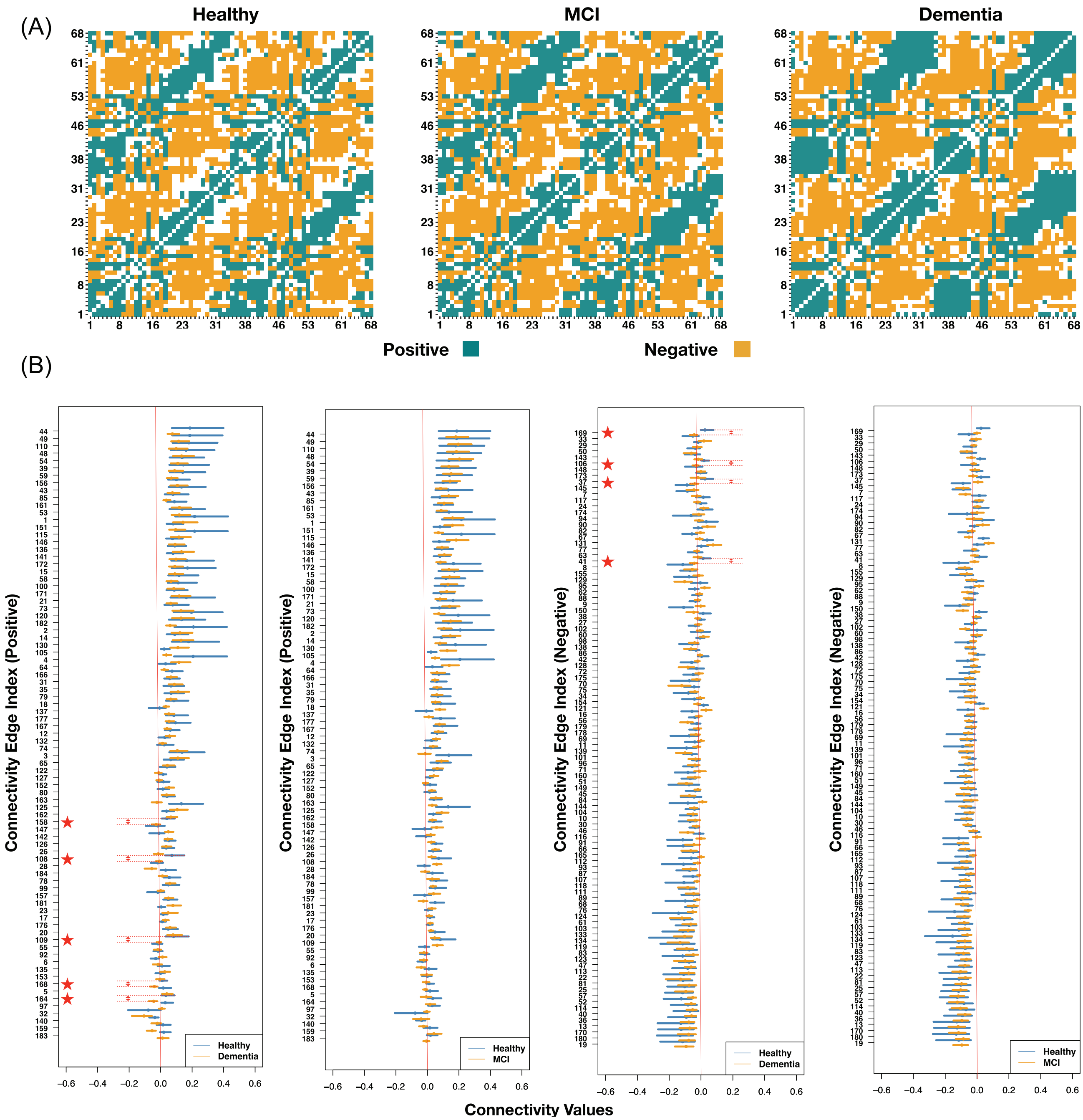

FIGURE 1 (A) A model estimated whole-brain functional connectivity networks for healthy (left), MCI (middle), and dementia patients (right) using male participants. Green indicates the presence of positive functional coactivation between a pair of brain regions, and yellow indicates the presence of negative functional co-activation between a pair of brain regions. (B) Based on male participants, we compare the 95% credible intervals of positive connectivity edges between healthy and dementia (leftmost), of positive connectivity edges between healthy and MCI (left middle), of negative connectivity edges between healthy and dementia (right middle) and of negative connectivity edges between healthy and MCI (rightmost). Connectivity edges are ranked by the intensity of the connections; large positive edges are ranked high on the *y*-axis and large negative edges are ranked low on the *y*-axis based on the baseline healthy female participants. Significant differences are highlighted in red. MCI, mild cognitive impairment.

the 95% CIs for healthy and MCI/dementia participants. This was derived from the posterior distributions for connectivity edges, given the data and our prior knowledge. This highlights the brain structures that are significantly different between healthy and MCI or dementia participants, which have the potential to guide the future development of neuroimaging biomarkers. For each clinical group, the 95% CI for the estimated connectivity was obtained from their posterior distributions with our proposed algorithm: the true connectivity value falls in this interval with 95% probability. Larger heterogeneity in connectivity edge estimates was found among healthy participants than

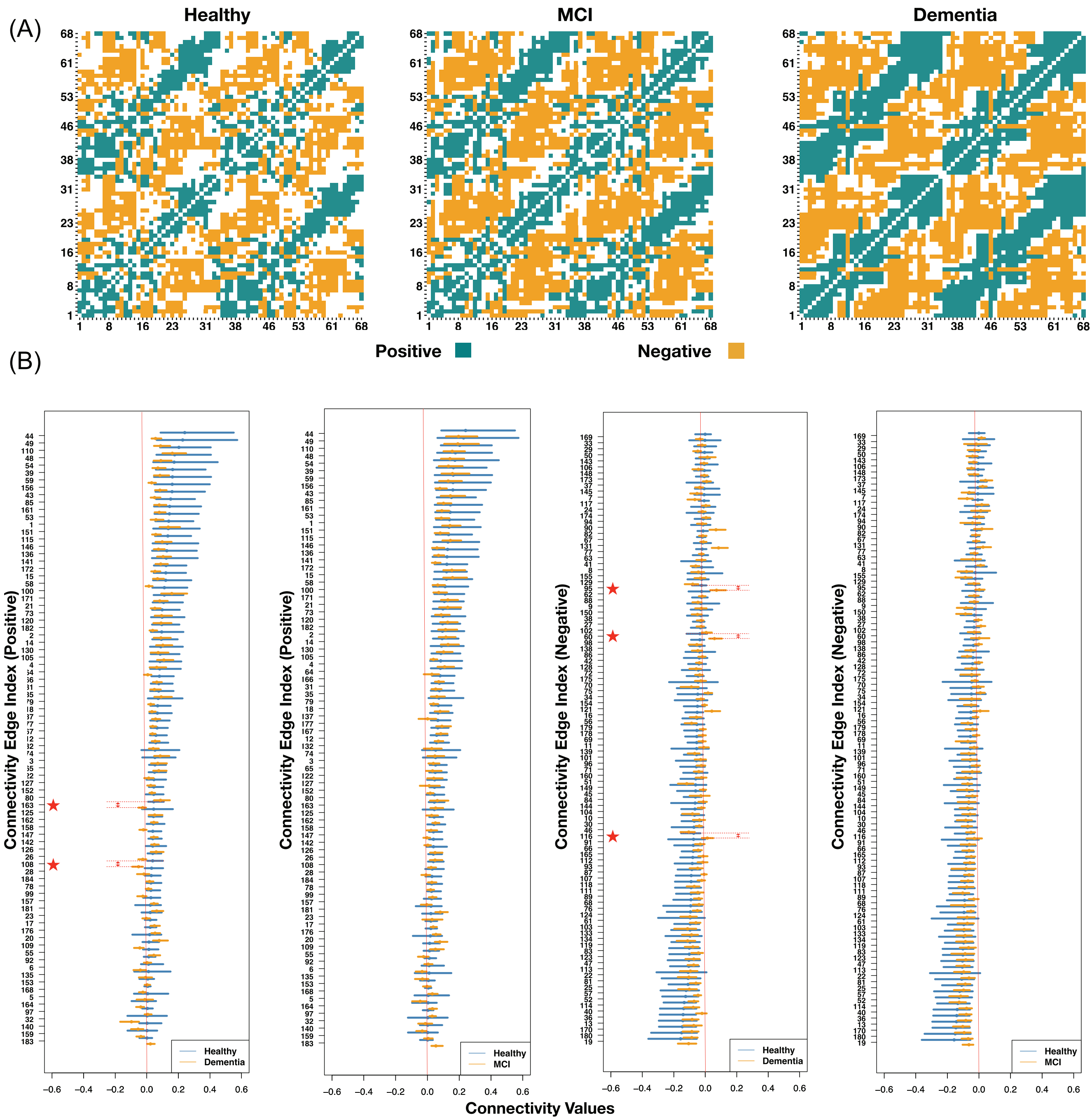

FIGURE 2 (A) A model estimated whole-brain functional connectivity networks for healthy (left), MCI (middle), and dementia patients (right) using female participants. Green indicates the presence of positive functional co-activation between a pair of brain regions, and yellow indicates the presence of negative functional co-activation between a pair of brain regions. (B) Based on female participants, we compare the 95% credible intervals of positive connectivity edges between healthy and dementia (leftmost), of positive connectivity edges between healthy and MCI (left middle), of negative connectivity edges between healthy and dementia (right middle) and of negative connectivity edges between healthy and MCI (rightmost). Connectivity edges are ranked by the intensity of the connections; large positive edges are ranked high on the *y*-axis and large negative edges are ranked low on the *y*-axis based on the baseline healthy female participants. Significant differences are highlighted in red. MCI, mild cognitive impairment.

MCI and dementia patients, particularly between regions with strong connections, for both positive and negative connectivity edges. In Figure 1B and Figure 2B, healthy participants tended to show wider 95% CIs than MCI and dementia patients, which suggests that there is a higher level of heterogeneity in functional connectivity among healthy participants than among MCI and dementia patients. At the same time, the intervals were notably wider for edges with larger magnitude and narrower for null edges whose strength are estimated to be close to zero. This differentiation is present for both males and female participants, and for healthy, MCI, and dementia patients. However, the differences are more evident in healthy participants. Meanwhile, perhaps unsurprisingly, Figure 1 and Figure 2 showed mostly consistent whole-brain functional connectivity networks between males and females with localized differences. Overall, edges that tended to have large positive estimates for males also tended to have large positive estimates for females with exceptions. For example, connectivity edges 1, 115, 172, and 15 in Figure 1B were more strongly connected in males than in females. We further explored these differences in the next section.

Based on healthy female subjects, we found significant associations between cortical volume and average thickness (95% CI of [0.3197, 0.8207]), average thickness and surface area (95% CI of [0.4748, 0.9963]), average thickness and PET (95% CI of [0.4917, 0.9977]), average thickness and PET (95% CI of [0.9936,1.0000]). This result was consist across all six groups.

In Figure 1, we found significant hyperactivity associated with dementia compared with healthy participants in five connectivity edges for males and significant hypoactivity associated with dementia compared with healthy participants in four connectivity edges for males. In Figure 2, we found significant hyperactivity associated with dementia compared with healthy participants in three connectivity edges for females and significant hypoactivity associated with dementia compared with healthy participants in two connectivity edges for females. Compared with males, females tended to experience significant changes in connectivity associated with the edges that have strong connectivity, a finding that was further illustrated.

3.1.2 | Dementia-associated dysfunction shows sex-based differences in location

To investigate dementia-associated changes in functional connectivity, we performed case–control comparisons, where we compared the estimated group-level connectivity for the healthy participants against the connectivity for dementia patients and people with MCI. We performed this analysis separately for males and females in Figure 3 and Figure 4. Similarly for males and females, we found overall less intense and more local changes in functional connectivity in MCI participants than dementia patients. Compared to healthy participants, dementia patients exhibited changes in functional connectivity across the whole brain (Figures 3A and 4A), whereas more local changes were found in MCI participants (Figures 3B and 4B).

In Figures 3B and 4B, we found differences in the locations of the functional changes associated with the development of MCI between males and females. For male and female MCI participants, we observed more consistent loss of connectivity within each functional circuit than between, which was also true for dementia patients. Between male and female MCI participants, more loss was observed in the somatomotor functional circuit for males, and more loss was observed in the visual system for females. To further pinpoint these changes in anatomical locations, we provide a visualization of the changes across the whole brain grouped by the anatomical lobes in the Supplementary Materials. Between male and female MCI participants, we found a stronger loss of functional connectivity in regions of the occipital lobe for females than for males. Both males and females experienced strong loss of functional activity in the occipital lobe during the dementia phase. Another region showing notable sex-based differences in functional connectivity changes was the parietal lobe. We found regions of the parietal lobe to be overly active for female dementia patients, but they showed neural or slightly less activity for male dementia patients. Overall, we found sex-based differences in functional connectivity neurodegeneration between males and females, which showed a potential link with our previous investigation of structural connectivity neurodegeneration identifying occipital and parietal lobe regions differences in the deterioration of white matter fiber tracks.[39] The mechanism behind the functional and structural changes in neurodegeneration is unclear at this point, and future studies are needed.

3.1.3 | An imbalance between excitatory and inhibitory mechanisms leads to whole-brain destabilization in dementia patients

We found decrease in network segregation associated with neurodegeneration, building on a previous work showing decrease in segregation associated with aging.[25] We report statistically significant changes in functional connectivity associated with dementia for females (Figure 5A) and males (Figure 5C), and we look at the distribution of the significant changes across functional circuits for females (Figure 5B) and males (Figure 5D). Statistical significance was established by taking into account uncertainty of the connectivity estimates in their posterior distributions under the Bayesian paradigm. For both males and females, with the development of dementia, there was a loss of intra-network functional connectivity while inter-network functional connections exhibited overactivation. This suggests an overall loss of network segregation with dementia, where stronger connectivity between functional circuits emerges with weaker connectivity within each functional circuit. This whole-brain system change indicates an imbalance between neural firing and synaptic plasticity, which can further contribute to neurodegeneration and cognitive impairment.[20,21,28]

In addition, we found differences between males and females in their excitatory or inhibitory imbalances associated with dementia. For females, DMN seems to be a key in both hypoactivity and hyperactivity in dementia. For males, we see hypoactivity concentrated with DMN and its connected circuits, but in terms of hyperactivity, we see stronger changes in LS than in DMN. In addition to DMN and LS, we also see frontoparietal (FP) and ventral attention (VA) systems implicated in dementia. Our results build onto existing literature demonstrating key roles that LS and DMN play in neurodegeneration, as well as provide new evidence for sex-based differences in dysfunction associated with dementia and whole-brain destabilization.

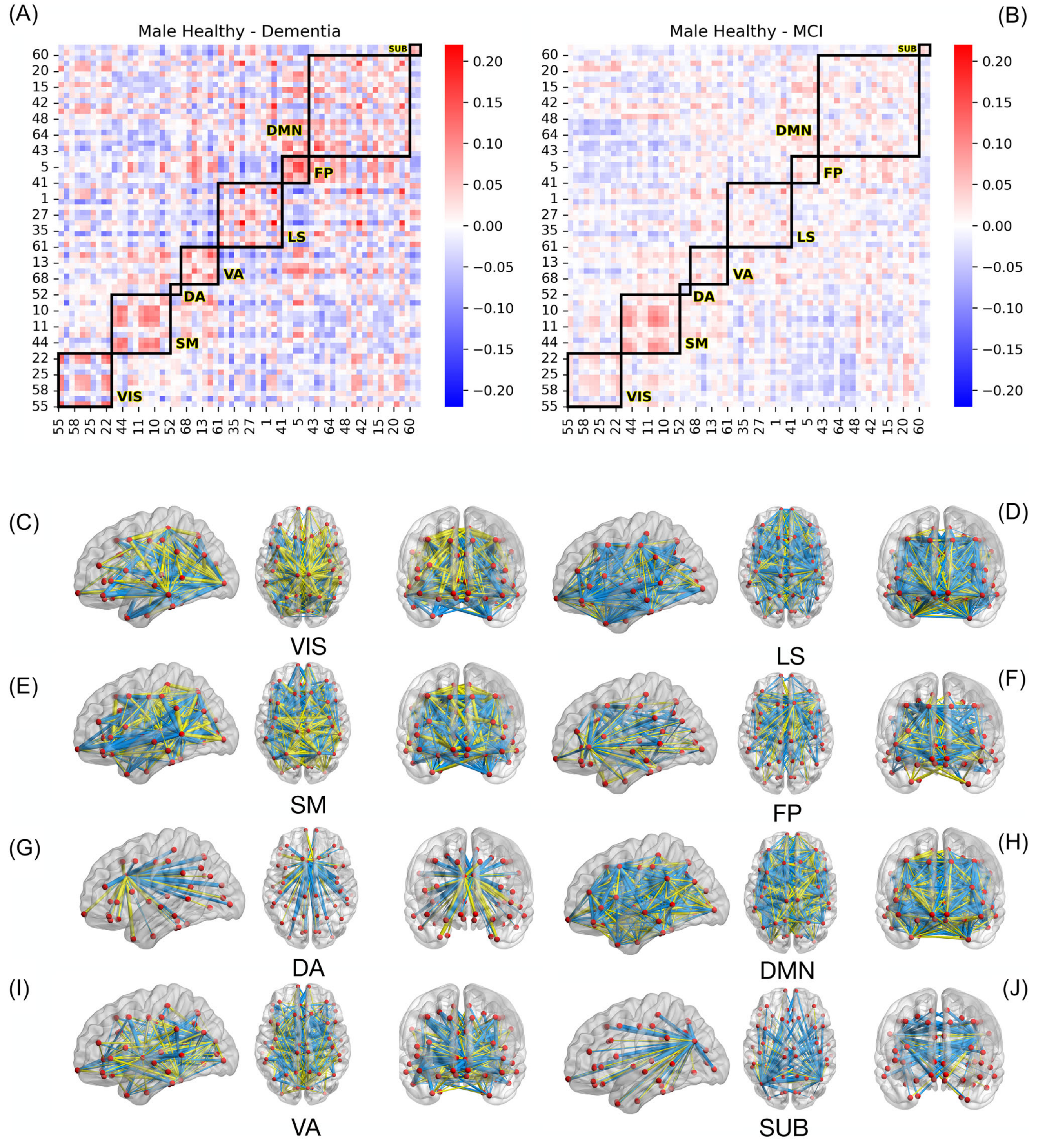

FIGURE 3 Estimated connectivity difference between healthy males and dementia males (A) and between healthy males and MCI males (B). The connectivity difference between healthy males and dementia males in functional systems (blue: dementia > healthy; yellow: healthy < dementia): visual system (C), LS (D), somatomotor (E), frontalparietal (F), dorsal attention (G), DMN (H), visual association (I), and subcortical (J). DMN, default mode network; LS, limbic system; MCI, mild cognitive impairment.

3.1.4 | Stronger links are found between centrality and neurodegeneration in females than in males

Last, we investigated the role of brain region centrality in neurodegeneration. Between males and females, regions with high node centralities in females also showed high centralities in males, although females had a wider range of centralities across the whole brain than males (Figure 6A and Figure 6B). The centrality is defined as the row sums of the positive or negative connectivity in the reference matrices, healthy female and healthy male groups, respectively. More specifically,

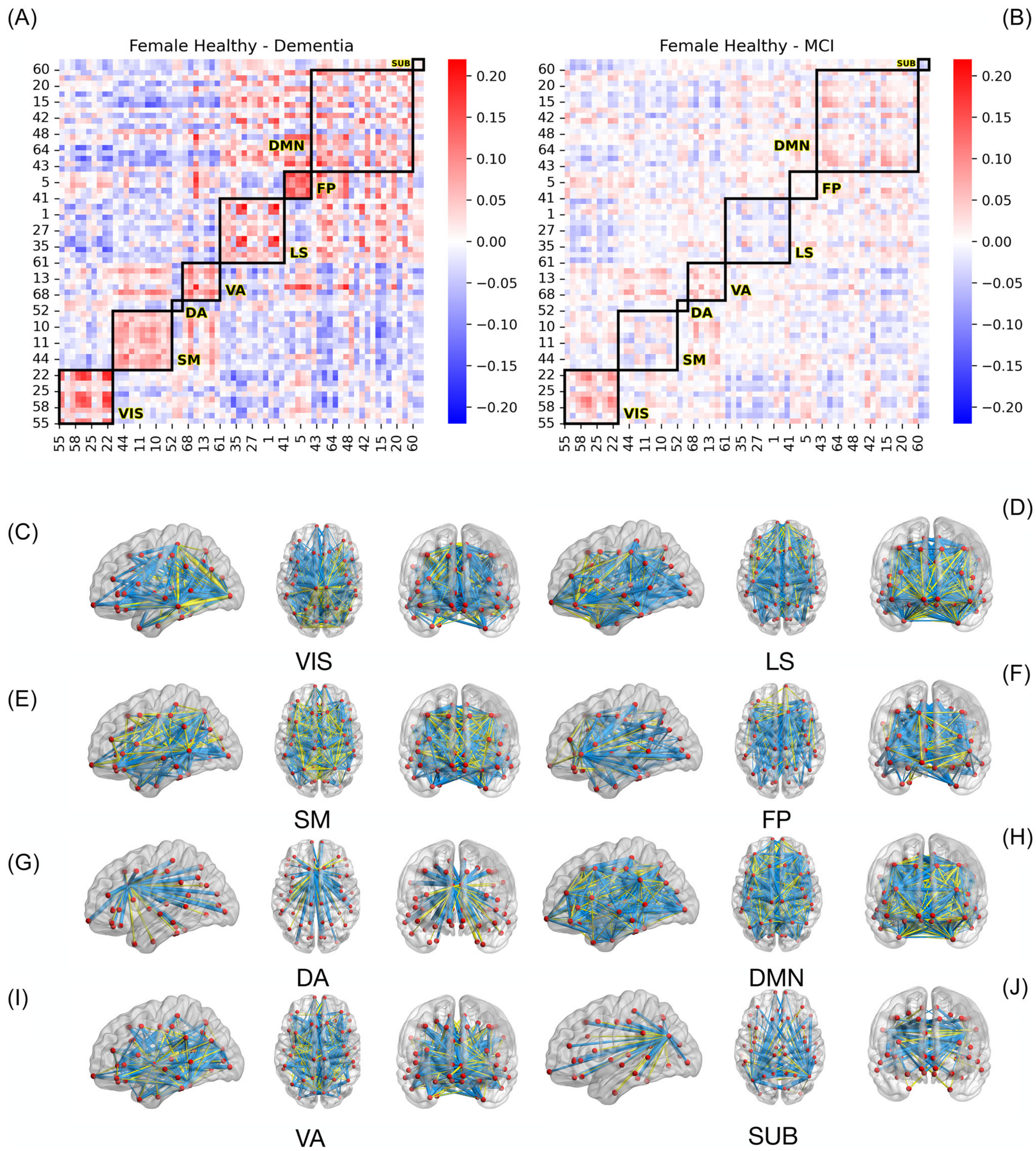

FIGURE 4 Estimated connectivity difference between healthy females and dementia females (A) and between healthy females and MCI females (B). The connectivity difference between healthy females and dementia females in functional systems (blue: dementia > healthy; yellow: healthy < dementia): visual system (C), LS (D), somatomotor (E), frontalparietal (F), dorsal attention (G), DMN (H), visual association (I), and subcortical (J). DMN, default mode network; LS, limbic system; MCI, mild cognitive impairment.

female subjects possessed extremely active regions, and females had more brain regions with centralities larger than 0.16 compared to males (Figure 6A). This differentiation between males and females is replicated with centralities based on negative functional edges but to a lesser degree.

For both females and males, changes in positive functional connectivity edges tended to have positive associations with centralities (Figure 6A), with females showing stronger associations than males. For negative functional edges, the differences between healthy and patient populations tended to have negative

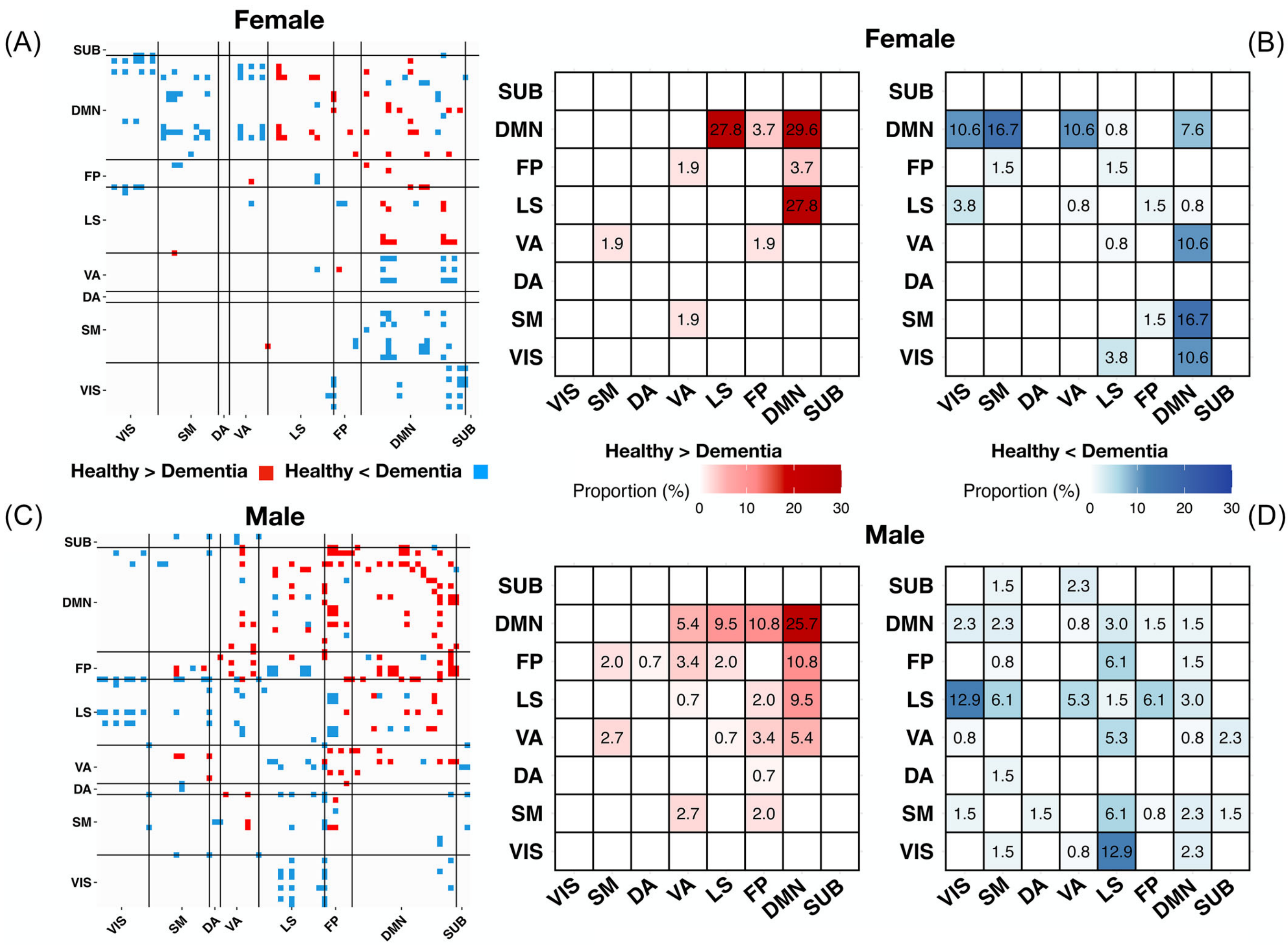

FIGURE 5 Statistically significant changes in functional connectivity with female (A) and male (C) dementia patients, compared to healthy participants across the whole brain. Red indicates a significant loss of functional connectivity associated with dementia, and blue indicates significantly overactive functional connectivity associated with dementia. We also show the proportion of significant changes found in each functional circuit and between each pair of functional circuits out of all significant changes for females (B) and males (D).

associations with centralities in the female population, but with no or mixed relationships in the male population. Overall, dementia effects tended to be larger for central actors of the network, and this finding was more consistent in the female population than in the male population. In Figure 6C, we see that, for both females and males, there were differences in brain connectivity among healthy-less-than-dementia, nonsignificant, and healthy-stronger-than-dementia functional imaging biomarkers, but the differentiation is less obvious for males. For females, strong connectivity edges tended to be affected by dementia, whereas, for males, the trend was less obvious.

4 | DISCUSSION

In this study, we show that network topology plays an active role in neurodegeneration with evidence supporting the presence of an imbalance between excitatory and inhibitory mechanisms leading to whole-brain destabilization in dementia patients. Our results are consistent with the current literature pinpointing the critical role that DMN plays in typical AD dementia[34–36] and confirm that both hypoactivity and hyperactivity are present in DMN with the development of dementia.[34,35] Furthermore, we find that females show more DMN-centered hyperactivity, whereas males show more LS-centered hyperactivity, while both show DMN-centered hypoactivity. We find that females, compared to males, exhibit stronger dementia-related changes in regions that are the central actors of the brain networks. Our study demonstrates the promise of uncovering the topological structure associated with pathologic aging and encourages future investigations of the underlying mechanisms between network structures and data modalities.

Our study extends the current knowledge about the sex differences in dementia and aging. Our study bridges together current knowledge about sex-based differences in key functional circuits such as DMN[27] and sex-based differences in "healthy" versus pathologic aging in terms of network segregation.[26] Evidence supports sex differences in key functional circuits such as DMN. DMN-associated intra- or

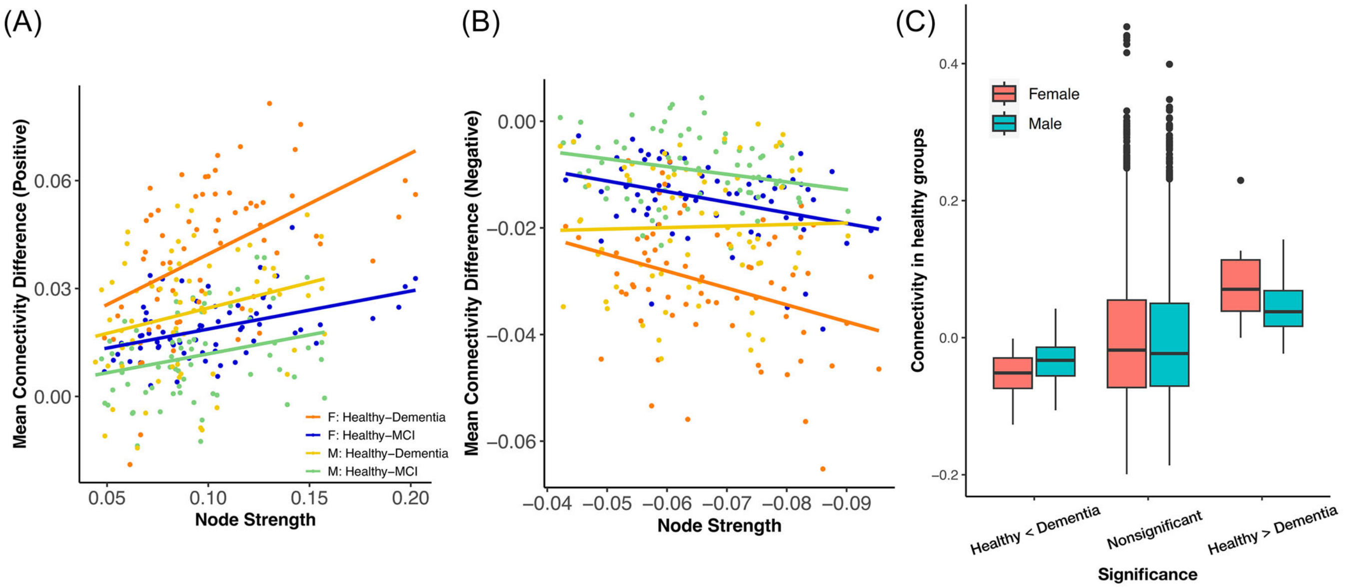

FIGURE 6 Mean connectivity difference between healthy and MCI/dementia participants as a function of node centrality for positive connectivity edges (A) and negative connectivity edges (B). We use healthy female participants as the baseline to calculate node centrality as well as to differentiate positive from negative functional connectivity edges. Boxplots of connectivity values for significant and non-significant imaging biomarkers (C). MCI, mild cognitive impairment.

internetwork hyperconnectivity has been associated with AD risk,[34,65] and progressive DMN hypoconnectivity has been associated with clinical AD illness.[35,36] Women, compared with men, have been found with higher connectivity with age in posterior DMN regions.[27]

Current research on sex differences in the aging brain shows differences in DMN functional connectivity, but this line of research is generally disconnected from investigations about the sex differences in topological changes in the brain, for example, changes in network segregation. Evidence supports that women rely more on between-circuit connectivity, and men show stronger modularity throughout aging.[67,68] Healthy aging women tend to show lower network segregation.[67]

Our study bridges these two theories together. Our results suggest that males and females show substantial differences in how dementia impacts brain functions. Males and females differ in dysfunction locations; females showed more DMN-centered hyperactivity, whereas males showed more LS-centered hyperactivity, while both showed DMN-centered hypoactivity. Furthermore, our study shows that these sex differences in functional connectivity occur simultaneously with changes in the topological structures of brain functional networks. We observe a stronger association between connectivity changes and regional centrality in females than in males. Our study uniquely contributes to the current literature by providing a more comprehensive picture of neurodegeneration linking centrality, network segregation, and DMN-centered changes in functional connectivity, and how these key components of neurodegeneration differ between the sexes.

Last, but not least, our study is significant because it highlights the disparity between males and females in typical AD dementia. Women, in addition to having a higher risk for developing typical AD dementia,[69] face a faster rate of pathology accumulation and more severe symptoms.[70,71] Given women's elevated risk for AD and increased longevity compared to men, understanding the etiology, pathophysiology, and progression of dementia in women and how they differ from men is critical for early detection and interventions, which could have a substantial impact on delaying or preventing dementia's devastating effects in people's daily lives as well as the sustainability of the healthcare system.

ACKNOWLEDGMENTS

Data collection and sharing for this project was funded by the Alzheimer's Disease Neuroimaging Initiative (ADNI) (National Institutes of Health Grant U01 AG024904) and DOD ADNI (Department of Defense award number W81XWH-12-2-0012). ADNI is funded by the National Institute on Aging, the National Institute of Biomedical Imaging and Bioengineering, and through generous contributions from the following: AbbVie, Alzheimer's Association; Alzheimer's Drug Discovery Foundation; Araclon Biotech; BioClinica, Inc.; Biogen; Bristol-Myers Squibb Company; CereSpir, Inc.; Cogstate; Eisai Inc.; Elan Pharmaceuticals, Inc.; Eli Lilly and Company; EuroImmun; F. Hoffmann-La Roche Ltd and its affiliated company Genentech, Inc.; Fujirebio; GE Healthcare; IXICO Ltd.; Janssen Alzheimer Immunotherapy Research & Development, LLC.; Johnson & Johnson Pharmaceutical Research & Development LLC.; Lumosity; Lundbeck; Merck & Co., Inc.; Meso Scale Diagnostics, LLC.; NeuroRx Research; Neurotrack Technologies; Novartis Pharmaceuticals Corporation; Pfizer Inc.; Piramal Imaging; Servier; Takeda Pharmaceutical Company; and Transition Therapeutics. The Canadian Institutes of Health Research is providing funds to support ADNI clinical sites in Canada. Private sector contributions are facilitated by the Foundation for the National Institutes of Health (www.fnih.org). The grantee organization is the Northern California

Institute for Research and Education, and the study is coordinated by the Alzheimer's Therapeutic Research Institute at the University of Southern California. ADNI data are disseminated by the Laboratory for Neuro Imaging at the University of Southern California. This study was supported in part by NIH grants RF1AG081413, RF1AG068191, R01EB034720, and P30AG066508.

CONFLICT OF INTEREST STATEMENT

The authors declare no conflict of interest. Author disclosures are available in the Supporting Information.

CONSENT STATEMENT

Consent was not necessary.

ORCID

Selena Wang https://orcid.org/0000-0002-4358-5382

REFERENCES

1. Alzheimer'sAssociation. 2024 Alzheimer's disease facts and figures. *Alzheimers Dement*. 2024;20:3708-3821.
2. Agüero-Torres H, Fratiglioni L, Guo Z, Viitanen M, Winblad B. Prognostic factors in very old demented adults: a seven-year follow-up from a population-based survey in Stockholm. *J Am Geriatr Soc*. 1998;46(4):444-452.
3. Tschanz JT, Corcoran CD, Schwartz S, et al. Progression of cognitive, functional, and neuropsychiatric symptom domains in a population cohort with Alzheimer dementia: the Cache County Dementia Progression study. *Am J Geriatr Psychiatry*. 2011;19(6):532-542.
4. Seeley WW, Crawford RK, Zhou J, Miller BL, Greicius MD. Neurodegenerative diseases target large-scale human brain networks. *Neuron*. 2009;62(1):42-52.
5. Pearson RC, Esiri MM, Hiorns RW, Wilcock GK, Powell TP. Anatomical correlates of the distribution of the pathological changes in the neocortex in Alzheimer disease. *Proc Natl Acad Sci USA*. 1985;82(13):4531-4534.
6. Saper CB, Wainer BH, German DC. Axonal and transneuronal transport in the transmission of neurological disease: potential role in system degenerations, including Alzheimer's disease. *Neuroscience*. 1987;23(2):389-398.
7. Braak H, Braak E. Neuropathological stageing of Alzheimer-related changes. *Acta Neuropathol*. 1991;82(4):239-259.
8. Jones DT, Graff-Radford J, Lowe VJ, et al. Tau, amyloid, and cascading network failure across the Alzheimer's disease spectrum. *Cortex*. 2017;97:143-159.
9. Vogel JW, Corriveau-Lecavalier N, Franzmeier N, et al. Connectome-based modelling of neurodegenerative diseases: towards precision medicine and mechanistic insight. *Nat Rev Neurosci*. 2023;24(10):620-639.
10. Franzmeier N, Rubinski A, Neitzel J, et al. Functional connectivity associated with tau levels in ageing, Alzheimer's, and small vessel disease. *Brain*. 2019;142(4):1093-1107.
11. Cope TE, Rittman T, Borchert RJ, et al. Tau burden and the functional connectome in Alzheimer's disease and progressive supranuclear palsy. *Brain*. 2018;141(2):550-567.
12. Franzmeier N, Neitzel J, Rubinski A, et al. Functional brain architecture is associated with the rate of tau accumulation in Alzheimer's disease. *Nat Commun*. 2020;11(1):347.
13. Franzmeier N, Dewenter A, Frontzkowski L, et al. Patient-centered connectivity-based prediction of tau pathology spread in Alzheimer's disease. *Sci Adv*. 2020;6(48):eabd1327.
14. Grothe MJ, Teipel SJ; Alzheimer's Disease Neuroimaging Initiative. Spatial patterns of atrophy, hypometabolism, and amyloid deposition in Alzheimer's disease correspond to dissociable functional brain networks. *Hum Brain Mapp*. 2016;37(1):35-53.
15. Pereira JB, Ossenkoppele R, Palmqvist S, et al. Amyloid and tau accumulate across distinct spatial networks and are differentially associated with brain connectivity. *ELife*. 2019;8:e50830.
16. Buckner RL, Sepulcre J, Talukdar T, et al. Cortical hubs revealed by intrinsic functional connectivity: mapping, assessment of stability, and relation to Alzheimer's disease. *J Neurosci*. 2009;29(6):1860-1873.
17. Buckner RL, Snyder AZ, Shannon BJ, et al. Molecular, structural, and functional characterization of Alzheimer's disease: evidence for a relationship between default activity, amyloid, and memory. *J Neurosci*. 2005;25(34):7709-7717.
18. Palmqvist S, Schöll M, Strandberg O, et al. Earliest accumulation of β-amyloid occurs within the default-mode network and concurrently affects brain connectivity. *Nat Commun*. 2017;8(1):1214.
19. Schöll M, Ossenkoppele R, Strandberg O, et al. Distinct 18F-AV-1451 tau PET retention patterns in early-and late-onset Alzheimer's disease. *Brain*. 2017;140(9):2286-2294.
20. Frere S, Slutsky I. Alzheimer's disease: from firing instability to homeostasis network collapse. *Neuron*. 2018;97(1):32-58.
21. Styr B, Slutsky I. Imbalance between firing homeostasis and synaptic plasticity drives early-phase Alzheimer's disease. *Nat Neurosci*. 2018;21(4):463-473.
22. Liu X, Li D, Ma M, Szymanski BK, Stanley HE, Gao J. Network resilience. *Phys Rep*. 2022;971:1-108.
23. Najjar W, Gaudiot J-L. Network resilience: a measure of network fault tolerance. In: IEEE Transactions on Computers. 1990;39(2):174-181.
24. Newman M. *Networks*. Oxford University Press; 2018.
25. Sun L, Zhao T, Liang X, et al. Functional connectome through the human life span. *Biorxiv*. 2024. https://www.ncbi.nlm.nih.gov/pmc/articles/PMC10515818/
26. Ju S, Horien C, Shen X, et al. Connectome-based predictive modeling shows sex differences in brain-based predictors of memory performance. *Front Dement*. 2023;2:1126016.
27. Ficek-Tani B, Horien C, Ju S, et al. Sex differences in default mode network connectivity in healthy aging adults. *Cereb Cortex*. 2023;33(10):6139-6151.
28. Busche MA, Konnerth A. Neuronal hyperactivity—a key defect in Alzheimer's disease?. *Bioessays*. 2015;37(6):624-632.
29. Faskowitz J, Yan X, Zuo XN, Sporns O. Weighted stochastic block models of the human connectome across the life span. *Sci Rep*. 2018;8(1):12997.
30. Chen T, et al. 'Bayesian subtyping for multi-state brain functional connectome with application on adolescent brain cognition'. *arXiv*. In: arXiv preprint arXiv:2302.10324. 2023.
31. Wang S, Constable T, Zhang S, Zhao Y. Heterogeneity analysis on multi-state brain functional connectivity and adolescent neurocognition. *J Am Statist Assoc*. 2024:1-21.
32. Hansson O, Grothe MJ, Strandberg TO, et al. Tau pathology distribution in Alzheimer's disease corresponds differentially to cognition-relevant functional brain networks. *Front Neurosci*. 2017;11:167.
33. Bassett DS, Zurn P, Gold JI. On the nature and use of models in network neuroscience. *Nat Rev Neurosci*. 2018;19(9):566-578.
34. Mormino EC, Smiljic A, Hayenga AO, et al. Relationships between beta-amyloid and functional connectivity in different components of the default mode network in aging. *Cereb Cortex*. 2011;21(10):2399-2407.
35. Greicius MD, Srivastava G, Reiss AL, Menon V. Default-mode network activity distinguishes Alzheimer's disease from healthy aging: evidence from functional MRI. *Proc Natl Acad Sci*. 2004;101(13):4637-4642.
36. Sheline YI, Raichle ME, Snyder AZ, et al. Amyloid plaques disrupt resting state default mode network connectivity in cognitively normal elderly. *Biol Psychiatry*. 2010;67(6):584-587.

37. Brier MR, Thomas JB, Snyder AZ, et al. Loss of intranetwork and internetwork resting state functional connections with Alzheimer's disease progression. *J Neurosci*. 2012;32(26):8890-8899.
38. Ossenkoppele R, Iaccarino L, Schonhaut DR, et al. Tau covariance patterns in Alzheimer's disease patients match intrinsic connectivity networks in the healthy brain. *NeuroImage Clin*. 2019;23:101848.
39. Wang S, Wang Y, Xu FH, Shen L, Zhao Y; Yize and Alzheimer's Disease Neuroimaging Initiative and others. Establishing group-level brain structural connectivity incorporating anatomical knowledge under latent space modeling. *Med Image Anal*. 2025;99:103309.
40. Weiner MW, Veitch DP, Aisen PS; Alzheimer's Disease Neuroimaging Initiative, et al. The Alzheimer's Disease Neuroimaging Initiative 3: continued innovation for clinical trial improvement. *Alzheimers Dement*. 2017;13(5):561-571. doi:10.1016/j.jalz.2016.10.006
41. Landau SM, Thomas BA, Thurfjell L, et al. Amyloid PET imaging in Alzheimer's disease: a comparison of three radiotracers. *Eur J Nucl Med Mol Imaging*. 2014;41:1398-1407.
42. Landau SM, Fero A, Baker SL, et al. Measurement of longitudinal β-amyloid change with 18F-florbetapir PET and standardized uptake value ratios. *J Nucl Med*. 2015;56(4):567-574.
43. Royse SK, Minhas DS, Lopresti BJ, et al. Validation of amyloid PET positivity thresholds in centiloids: a multisite PET study approach. *Alzheimers Res Ther*. 2021;13(1):99.
44. Xu F, Garai S, Duong-Tran D, et al. Consistency of graph theoretical measurements of Alzheimer's disease fiber density connectomes across multiple parcellation scales. In: *(BIBM) 2022 IEEE International Conference on Bioinformatics and Biomedicine* IEEE Regular Paper. 2022;2022:1323-1328.
45. Tourbier S, Rue-Queralt J, Glomb K, et al. Connectome Mapper 3: a flexible and open-source pipeline software for multiscale multimodal human connectome mapping. *J Open Source Software*. 2022;7(74):4248. doi:10.21105/joss.04248
46. Cammoun L, Gigandet X, Meskaldji D, et al. Mapping the human connectome at multiple scales with diffusion spectrum MRI. *J Neurosci Methods*. 2012;203(2):386-397. doi:10.1016/j.jneumeth.2011.09.031
47. Cox RW. AFNI: software for analysis and visualization of functional magnetic resonance neuroimages. *Comput Biomed Res*. 1996;29(3):162-173.
48. Jenkinson M, Smith S. A global optimisation method for robust affine registration of brain images. *Med Image Anal*. 2001;5(2):143-156.
49. Jenkinson M, Bannister P, Brady M, Smith S. Improved optimization for the robust and accurate linear registration and motion correction of brain images. *Neuroimage*. 2002;17(2):825-841.
50. Yeo BT, Krienen FM, Sepulcre J, et al. The organization of the human cerebral cortex estimated by intrinsic functional connectivity. *J Neurophysiol*. 2011;106(3):1125-1165. doi:10.1152/jn.00338.2011
51. Klein A, Tourville J. 101 Labeled brain images and a consistent human cortical labeling protocol. *Front Neurosci*. 2012;6:171. https://www.frontiersin.org/journals/neuroscience/articles/10.3389/fnins.2012.00171
52. Brown JA, Lee AJ, Pasquini L, Seeley WW. A dynamic gradient architecture generates brain activity states. *Neuroimage*. 2022;261:119526.
53. Hong S-J, Xu T, Nikolaidis A, et al. Toward a connectivity gradient-based framework for reproducible biomarker discovery. *Neuroimage*. 2020;223:117322.
54. Lee CH, Park H, Lee MJ, Park BY. Whole-brain functional gradients reveal cortical and subcortical alterations in patients with episodic migraine. *Hum Brain Mapp*. 2023;44(6):2224-2233.
55. Lioi G, Gripon V, Brahim A, Rousseau F, Farrugia N. Gradients of connectivity as graph Fourier bases of brain activity. *Netw Neurosci*. 2021;5(2):322-336.
56. Becker CO, Pequito S, Pappas GJ, et al. Spectral mapping of brain functional connectivity from diffusion imaging. *Sci Rep*. 2018;8(1):1411.
57. Deslauriers-Gauthier S, Zucchelli M, Frigo M, Deriche R. A unified framework for multimodal structure–function mapping based on eigenmodes. *Med Image Anal*. 2020;66:101799.
58. Sosa J, Buitrago L. A review of latent space models for social networks. *Revista Colombiana de Estadstica*. 2021;44(1):171-200.
59. Hoff PD. Bilinear mixed-effects models for dyadic data. *J Am Statist Assoc*. 2005;100(469):286-295.
60. Hoff PD. Modeling homophily and stochastic equivalence in symmetric relational data. In: Platt J C, ed. *Advances in Neural Information Processing Systems 20*. MIT Press; 2008:657-664. arXiv:0711.1146.
61. Hoff P. Additive and multiplicative effects network models. *Statl Sci*. 2021;36(1):34-50.
62. Bassett DS, Bullmore ED. Small-world brain networks. *Neuroscientist*. 2006;12(6):512-523.
63. Gollini I, Murphy TB. Joint modeling of multiple network views. *J Comput Graph Statist*. 2016;25(1):246-265.
64. D'Angelo S, Murphy TB, Alfò M. Latent space modelling of multidimensional networks with application to the exchange of votes in Eurovision song contest. *Ann Appl Stat*. 2018. https://api.semanticscholar.org/CorpusID:88523060
65. Schultz AP, Chhatwal JP, Hedden T, et al. Phases of hyperconnectivity and hypoconnectivity in the default mode and salience networks track with amyloid and tau in clinically normal individuals. *J Neurosci*. 2017;37(16):4323-4331. https://www.jneurosci.org/content/37/16/4323
66. Hampton OL, Buckley RF, Manning LK, et al. Resting-state functional connectivity and amyloid burden influence longitudinal cortical thinning in the default mode network in preclinical Alzheimer's disease. *NeuroImage Clin*. 2020;28:102407.
67. Ingalhalikar M, Smith A, Parker D, et al. Sex differences in the structural connectome of the human brain. *Proc Natl Acad Sci USA*. 2014;111(2):823-828.
68. Rabipour S, Rajagopal S, Pasvanis S; PREVENT-AD Research Group, Rajah MN. Generalization of memory-related brain function in asymptomatic older women with a family history of late onset Alzheimer's disease: results from the PREVENT-AD Cohort. *Neurobiol Aging*. 2021;104:42-56.
69. *Dementia — who.int*. [Accessed 19-04-2024]. https://www.who.int/news-room/fact-sheets/detail/dementia
70. Barnes LL, Wilson RS, Bienias JL, Schneider JA, Evans DA, Bennett DA. Sex differences in the clinical manifestations of Alzheimer disease pathology. *Arch Gen Psychiatry*. 2005;62(6):685-691. https://jamanetwork.com/journals/jamapsychiatry/fullarticle/208641
71. Edwards L, La Joie R, Iaccarino L, et al. Multimodal neuroimaging of sex differences in cognitively impaired patients on the Alzheimer's continuum: greater tau-PET retention in females. *Neurobiol Aging*. 2021;105:86-98.

SUPPORTING INFORMATION

Additional supporting information can be found online in the Supporting Information section at the end of this article.

How to cite this article: Wang S, Wang Y, Xu FH, et al. Sex-specific topological structure associated with dementia via latent space estimation. *Alzheimer's Dement*. 2024;20:8387–8401. https://doi.org/10.1002/alz.14266